Available online at www.sciencedirect.com
SCIENCE DIRECT®
International Journal of Thermal Sciences 43 (2004) 135–144
International Journal of Thermal Sciences
www.elsevier.com/locate/ijts

Rayleigh–Bénard convection in tall rectangular enclosures

Maria Cappelli D'Orazio, Claudio Cianfrini, Massimo Corcione *

Dipartimento di Fisica Tecnica, Università di Roma "La Sapienza" via Eudossiana, 18-00184 Rome, Italy

Received 8 April 2003; accepted 23 May 2003

Abstract

Natural convection in air-filled, 2-D rectangular enclosures heated from below and cooled from above is studied numerically under the assumption of adiabatic sidewalls. A computational model based on the SIMPLE-C algorithm is used for solving the mass, momentum, and energy transfer governing equations. Simulations are performed for different values of the height-to-width aspect ratio of the enclosure in the range $2 \leqslant A \leqslant 6$, by progressively increasing and successively decreasing the Rayleigh number in the range $10^3 \leqslant Ra \leqslant 2 \times 10^6$. After the departure from motionless conduction takes place, the following flow-pattern evolution is detected: one-cell steady → two-cell steady → two-cell periodic → one-to-three-cell periodic → three-cell periodic. At each bifurcation, either abrupt or smooth changes in the Nusselt number are found to occur, according to whether the flow-transition is either sudden or more gradual. Hysteresis phenomena occurrence is documented. The effects of tilting the enclosure upon the stability of the different flow structures are also analysed.

Keywords: Rayleigh–Bénard convection; Tall rectangular enclosures; Flow-transitions; Multiple solutions; Tilting destabilizing effect

1. Introduction

Rayleigh–Bénard convection in confined enclosures has attracted considerable attention due to its practical relevance to many engineering and science applications, and to its theoretical interest as a convenient vehicle for the study of the dynamic behavior of non-linear systems. In particular, much effort has been dedicated to investigate both flow-instabilities and flow-transitions or bifurcations, i.e., changes in the spatio-temporal flow patterns with varying a control parameter, usually assumed to be the Rayleigh number of the enclosure.

A general well-known result obtained by many researchers is that a first bifurcation from motionless conduction to steady-state convection occurs as the Rayleigh number is increased beyond a critical value which depends on the aspect ratio of the enclosure (see, e.g., Raithby and Holland [1]). As the Rayleigh number is further increased, motion becomes unstable and subsequent flow-transitions lead to an increasing spatio-temporal complexity which ultimately results in turbulence. According to a typical bifurcation sequence, steady-state convection becomes at first oscillatory, then turning into quasi-periodic and eventually chaotic motion. The onset of chaos may then be followed by windows of periodicity, which emphasize the surprisingly complicated dynamic behavior of Rayleigh–Bénard systems. However, different routes to chaos and turbulence may be followed, according to the fact that bifurcation sequences are strong function of the thermal hystory of the system and of the step change in the Rayleigh number (see Gollub and Benson [2], Libchaber et al. [3], and Mukutmoni and Yang [4–6]). In addition, hysteresis effects were also reported (see, e.g., Leith [7]), thus confirming that the Rayleigh–Bénard problem, due to its non-linearity, is a degenerate problem, i.e., for the same set of governing parameters multiple solutions, each strongly dependent on the initial conditions, are possible. Flow-pattern evolutions of the same kind of those described above were detected also when the aspect ratio of the enclosure was assumed as control parameter instead of the Rayleigh number (see Hernandez and Frederick [8]). Detailed surveys of Rayleigh–Bénard convection, as well as reviews on the several studies conducted, are widely available in the open literature (see, e.g., Yang [9], Koschmieder [10], Getling [11], and Gelfgat [12]).

Despite the enormous amount of experimental, theoretical, and numerical studies performed on this topic, it seems worthwhile noticing that most of the work done deals mainly

* Corresponding author.
E-mail address: massimo.corcione@uniroma1.it (M. Corcione).

1290-0729/$ – see front matter
doi:10.1016/j.ijthermalsci.2003.05.002

Nomenclature

A	height-to-width aspect ratio of the enclosure, $= H/L$		
g	gravitational acceleration	9.81	m·s^{-2}
H	height of the enclosure		m
h	average coefficient of convection		W·m^{-2}·K^{-1}
k	thermal conductivity of the fluid		W·m^{-1}·K^{-1}
L	length of the enclosure		m
Nu	average Nusselt number, $= hH/k$		
P	dimensionless pressure		
p	pressure		Pa
Pr	Prandtl number, $= \nu/\alpha$		
Q	heat transfer rate		W
Ra	Rayleigh number based on the height of the cavity, $= g\beta(T_h - T_c)H^3/\alpha\nu$		
T	period of oscillation		s
T	temperature		K
T_0	reference temperature		K
t	time		s
U	dimensionless horizontal velocity component		
V	dimensionless vertical velocity component		
u	horizontal velocity component		m·s^{-1}
v	vertical velocity component		m·s^{-1}
X	dimensionless horizontal coordinate		
Y	dimensionless vertical coordinate		
x	horizontal coordinate		m
y	vertical coordinate		m

Greek symbols

α	thermal diffusivity of the fluid		m^2·s^{-1}
β	coefficient of volumetric thermal expansion of the fluid		K^{-1}
ν	kinematic viscosity of the fluid		m^2·s^{-1}
θ	dimensionless temperature		
ρ	density of the fluid		kg·m^{-3}
τ	dimensionless time		
Ψ	dimensionless stream function		

Subscripts

av	average
c	cold, referred to the top wall
h	hot, referred to the bottom wall
max	maximum value
0	evaluated at the reference temperature

with cavities extensive in the horizontal direction, i.e., cavities whose height is significantly smaller than the other dimensions. In contrast, only few studies were carried out for aspect ratios close or equal to unity (see Pallares et al. [13, 14]), whilst a considerably smaller attention has been dedicated to tall cavities, i.e., cavities heated from below which extend in the vertical direction.

In this framework, aim of the present paper is to carry out a first-approach numerical analysis of the Rayleigh–Bénard convection in tall, two-dimensional enclosures filled with air. Indeed, the analysis performed here must be intended as a preliminar study of the dynamic behavior of real slender cavities heated from below, being reasonable to expect that the thermal convection inside tall three-dimensional cavities may also be dominated by three-dimensional effects, as in the real bottom-heated horizontal enclosures (where, besides the quasi two-dimensional transverse and longitudinal rolls, the formation of typically three-dimensional cross-roll and soft-roll flow structures may occur).

The analysis is conducted under the assumption of laminar flow, for different values of both the height-to-width aspect ratio of the enclosure in the range between 2 and 6, and the Rayleigh number based on the height of the cavity in the range between 10^3 and 2×10^6. Major concern of the work is to study the evolution of the heat transfer features of the enclosure, to document and discuss the bifurcations that occur as the Rayleigh number is progressively either increased or decreased within its range of variability, and to investigate the occurrence of hysteresis phenomena.

2. Physical and mathematical formulation

An air-filled rectangular enclosure of height H and width L is considered. The coordinate system is defined so that the x-axis is horizontal, whilst the y-axis is vertical and pointing upwards in the direction opposite to gravity. Constant uniform temperatures T_h and T_c (with $T_h > T_c$) are imposed at the bottom and top walls, respectively. The right and left sidewalls are assumed adiabatic. The geometry of the enclosure is depicted in Fig. 1(a), where the coordinate system and the thermal state of the boundary walls are also represented.

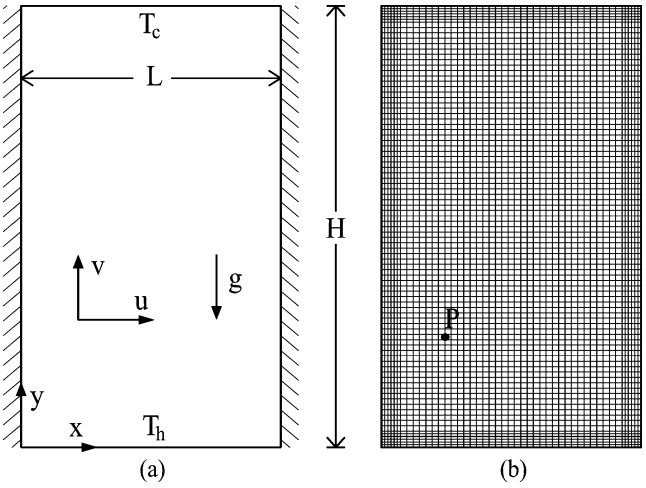

Fig. 1. Sketch of the geometry, coordinate system and discretization grid.

The flow is considered to be two-dimensional and laminar. The fluid is assumed to be incompressible, with constant physical properties and negligible viscous dissipation. The buoyancy effects upon momentum transfer are taken into account through the Boussinesq approximation.

Once the above assumptions are employed in the conservation equations of mass, momentum, and energy, and the following dimensionless variables are introduced:

$$X = \frac{x}{H}, \qquad Y = \frac{y}{H}, \qquad \tau = \frac{t}{(H^2/\nu)} \tag{1}$$

$$U = \frac{u}{(\nu/H)}, \qquad V = \frac{v}{(\nu/H)}, \qquad P = \frac{p + \rho_0 g y}{\rho(\nu/H)^2} \tag{2}$$

$$\theta = \frac{(T - T_0)}{(T_\mathrm{h} - T_\mathrm{c})} \quad \text{with } T_0 = (T_\mathrm{h} + T_\mathrm{c})/2 \tag{3}$$

the following set of governing equations is obtained:

$$\frac{\partial U}{\partial X} + \frac{\partial V}{\partial Y} = 0 \tag{4}$$

$$\frac{\partial U}{\partial \tau} + U\frac{\partial U}{\partial X} + V\frac{\partial U}{\partial Y} = -\frac{\partial P}{\partial X} + \left(\frac{\partial^2 U}{\partial X^2} + \frac{\partial^2 U}{\partial Y^2}\right) \tag{5}$$

$$\frac{\partial V}{\partial \tau} + U\frac{\partial V}{\partial X} + V\frac{\partial V}{\partial Y} = -\frac{\partial P}{\partial Y} + \left(\frac{\partial^2 V}{\partial X^2} + \frac{\partial^2 V}{\partial Y^2}\right) + \frac{Ra}{Pr}\theta \tag{6}$$

$$\frac{\partial \theta}{\partial \tau} + U\frac{\partial \theta}{\partial X} + V\frac{\partial \theta}{\partial Y} = \frac{1}{Pr}\left(\frac{\partial^2 \theta}{\partial X^2} + \frac{\partial^2 \theta}{\partial Y^2}\right) \tag{7}$$

where $Ra = g\beta(T_\mathrm{h} - T_\mathrm{c})H^3/\alpha\nu$ is the Rayleigh number based on the height of the enclosure and $Pr = \nu/\alpha$ is the Prandtl number, set to 0.71.

The thermal boundary conditions assumed at the walls are: (a) $\theta = +0.5$ at the bottom wall, $Y = 0$; (b) $\theta = -0.5$ at the top wall, $Y = 1$; and (c) $\partial\theta/\partial X = 0$ at the left and right sidewalls, $X = 0$ and $X = 1/A$, respectively, where $A = H/L$ is the aspect ratio of the enclosure. The no-slip boundary condition $U = V = 0$ is then imposed at the four walls of the cavity. As initial conditions, the results obtained at a given Rayleigh number are successively used for computations at higher or lower Rayleigh numbers, as clarified in the next section of the paper. Additional simulations are also performed with the following initial conditions:

(a) fluid at rest and conductive linear temperature distribution;
(b) fluid at rest and uniform temperature $\theta = -0.5$, or $\theta = 0$, or $\theta = +0.5$ across the cavity.

3. Computational procedure

The system of Eqs. (4)–(7) with the boundary conditions stated above is solved through a control-volume formulation of the finite-difference method. The pressure-velocity coupling is handled by using the SIMPLE-C algorithm by Van Doormaal and Raithby [15], which is essentially a more implicit variant of the SIMPLE algorithm by Patankar and Spalding [16]. The convective fluxes across the surfaces of the control volumes are evaluated by using the power-law discretization scheme recommended by Patankar [17]. A second-order backward scheme is then used for time stepping. Starting from specified initial values of the independent variables, i.e., specified initial temperature and velocity fields, at each time step the discretized governing equations are solved iteratively through a line-by-line application of the Thomas algorithm. Under-relaxation is used to ensure the convergence of the iterative procedure. Details on the SIMPLE procedure and on the discretization of the convective fluxes may be found in Patankar [17]. In addition, studies on the comparative performance of different discretization schemes for the evaluation of the interface convective fluxes, as well as studies on enhanced variants of the basic SIMPLE algorithm, are referenced and discussed in a general review paper by Patankar [18].

The computational spatial domain is covered with a non-equidistant grid, having a concentration of grid lines near the four walls of the cavity, and a uniform spacing throughout the remainder interior of the cavity. Time discretization is chosen uniform. Within each time step, the spatial solution is considered to be fully converged when the maximum absolute values of both the mass source and the percent changes of the independent variables at any grid-node from iteration to iteration are smaller than prescribed values, i.e., 10^{-4} and 10^{-5}, respectively. Time-integration is stopped once an asymptotic solution, either stationary or periodic, is reached. This means that the simulation procedure is halted when the percent difference between the incoming and outgoing heat transfer rates at the bottom and top walls, as well as the percent changes of the time-derivatives of the independent variables at any grid-node from time-step to time-step, are smaller than prescribed values, i.e., 10^{-6} and 10^{-7}, respectively. In addition, during each simulation performed, the dynamic behavior of the system analysed is followed by plotting the phase trajectories of θ, U, and V, at some fixed grid locations, i.e., by plotting the distributions of the time derivatives of the primitive variables versus the variables themselves with time as parameter, whose attractor may be represented by either a fixed point, or a limit cycle, or a torus, or a so-called strange attractor, according to whether a stationary, or an oscillatory, or a quasi-periodic, or a chaotic solution, respectively, is reached.

As concerns the initial conditions, most of the simulations are performed by progressively increasing or decreasing the Rayleigh number, as said above. In particular, since the highly non-linear problems such as this are very sensitive to the thermal hystory, and the occurrence of hysteresis phenomena is one of the main interests of the present study, the sequence of the numerical solutions, i.e., in what steps the Rayleigh number is increased or decreased between successive runs, must be clearly specified. In computations

wherein the Rayleigh number is increased, the flow and temperature fields relevant to the critical value Ra_C which corresponds to the onset of steady-state convection are first solved with the assumption that the initial velocity field is null and the initial temperature distribution across the cavity is linear between -0.5 and $+0.5$. These fields are then employed as the initial condition for the solution of the subsequent case with a Rayleigh number $Ra = Ra_C + \Delta Ra$, thus beginning a computational sequence which proceeds with a step change $\Delta Ra = 10^n$ for Rayleigh numbers in the range $10^n \leqslant Ra \leqslant 10^{n+1}$. Once the solution at the largest Rayleigh number investigated, i.e., 2×10^6 for $A = 2$ and 10^6 for $A > 2$, is obtained, the exploration procedure is reversed, which means that the Rayleigh number is progressively decreased by the same step changes ΔRa used in the "outward journey". At any bifurcation occurrence, a more refined step change in the range between one-tenth and one-fourth of the former ΔRa is employed, so as to locate the flow-transition with a better accuracy. This same step-refinement is used also to get a better resolution of the Nu-curves in the proximity of steep gradients and/or maximum points, when required.

At each time step, after spatial convergence is attained, the average Nusselt numbers Nu_h and Nu_c of the bottom and top walls, respectively, are calculated:

$$Nu_h = \frac{Q_h H}{kL(T_h - T_c)} = -A \int_0^{1/A} \frac{\partial\theta}{\partial Y}\Big|_{Y=0} dX \tag{8}$$

$$Nu_c = \frac{Q_c H}{kL(T_h - T_c)} = A \int_0^{1/A} \frac{\partial\theta}{\partial Y}\Big|_{Y=1} dX \tag{9}$$

where Q_h and Q_c are the heat transfer rates at the bottom and top walls, respectively. The temperature gradients at both bottom and top walls are evaluated by assuming a second-order temperature profile among each wall-node and the next two interior nodes. The integrals are then approximated by the trapezoid rule. Of course, once a steady-state solution is reached, the two average Nusselt numbers Nu_h and Nu_c coincide to what we could name the average Nusselt number Nu of the enclosure. This same coincidence occurs at any time interval also when a steady-periodic solution is reached. Whenever periodicity occurs, the heat transfer characteristics of the enclosure are expressed through an average Nusselt number defined as follows:

$$\begin{aligned} Nu &= -\frac{A}{10T} \int_0^{10T} \left(\int_0^{1/A} \frac{\partial\theta(\tau)}{\partial Y}\Big|_{Y=0} dX \right) d\tau \\ &= \frac{A}{10T} \int_0^{10T} \left(\int_0^{1/A} \frac{\partial\theta(\tau)}{\partial Y}\Big|_{Y=1} dX \right) d\tau \end{aligned} \tag{10}$$

where $10T$ are the last ten periods of oscillation computed by the solution algorithm.

Tests on the dependence of the results on both grid-size and time-step have been performed for all the geometrical configurations investigated, at several Rayleigh numbers. In particular, the optimal values of mesh spacing and time stepping, i.e., those used for computations, which represent a good compromise between solution accuracy and computational time required, are assumed as those over which further refinements do not produce any noticeable modification in both the predicted flow field and the heat transfer rates. This means that, at selected sampling physical times, the percent changes of the average Nusselt numbers Nu_h and Nu_c defined above, as well as those of the maximum horizontal and vertical velocity components on the two midplanes of the enclosure, must be smaller than prescribed accuracy values, i.e., 1% and 2–5%, respectively. Typically, the number of nodal points and the time stepping used for computations lie respectively in the range between 47×88 and 47×252, and in the range between 10^{-4} and 5×10^{-6}, depending on both the aspect ratio and the Rayleigh number of the enclosure investigated. As an example, the 47×88 discretization grid used for the enclosure with $A = 2$ is depicted in Fig. 1(b).

Furthermore, in order to validate the numerical code used for the present study, the steady-state solutions obtained as temporal asymptotic solutions in a square cavity with differentially heated sidewalls and adiabatic top and bottom walls for Rayleigh numbers in the range between 10^3 and 10^6, have been compared with the benchmark results obtained by de Vahl Davis through a standard finite-difference method used to solve the stream function-vorticity formulation of the governing equations [19]. In particular, the average Nusselt numbers throughout the cavity as well as the maximum horizontal and vertical velocity components, respectively on the vertical and the horizontal midplane of the enclosure, are within 1% of the benchmark data, as indicated in Table 1, where other reference solutions obtained by other authors

Table 1
Comparison of the thermally-driven square cavity solutions

Quantities	Benchmark [19]	Present work	FV [20,21]
		$Ra = 10^3$	
U_{max}	3.649	3.654	3.649
V_{max}	3.697	3.708	3.690
Nu_{av}	1.118	1.116	1.113
		$Ra = 10^4$	
U_{max}	16.178	16.242	16.180
V_{max}	19.617	19.714	19.629
Nu_{av}	2.243	2.254	2.244
		$Ra = 10^5$	
U_{max}	34.722	35.008	34.739
V_{max}	68.590	68.109	68.639
Nu_{av}	4.519	4.506	4.521
		$Ra = 10^6$	
U_{max}	64.630	65.226	64.836
V_{max}	219.360	221.598	220.461
Nu_{av}	8.800	8.879	8.825

through finite-volume methods are also reported (i.e., the results by Mahdi and Kinney [20], for $Ra = 10^3$, and those by Hortmann et al. [21], for $Ra = 10^4$ to 10^6). It seems worth noticing that our dimensionless velocity results have been multiplied by the Prandtl number before being inserted in Table 1, so as to account for the choice of the ratio between kinematic viscosity and characteristic length of the cavity as scale factor for the velocity, instead of the ratio between thermal diffusivity and characteristic length, used by de Vahl Davis in Ref. [19]. In addition, also the transient solutions found by Aydin [22] in air-filled square enclosures heated from one side and cooled from above at several Rayleigh numbers have been reproduced with rather good accuracy.

4. Results and discussion

Numerical simulations are performed for $Pr = 0.71$ (air is the working fluid) and different values of both the Rayleigh number in the range $10^3 \leqslant Ra \leqslant 10^6$ and the height-to-width aspect ratio of the cavity in the range $2 \leqslant A \leqslant 6$. A survey of the heat transfer and fluid flow overall results obtained is presented and discussed. Some local results are also reported by means of isotherm and streamline plots, where the contour lines correspond to equispaced values of respectively the dimensionless temperature θ in the range between -0.5 and $+0.5$ and the normalized dimensionless stream function $|\Psi|/|\Psi|_{\max}$ in the range between 0 and 1, being Ψ defined as usual through $U = \partial\Psi/\partial Y$ and $V = -\partial\Psi/\partial X$.

The evolution of the average Nusselt number of the enclosure and that of the flow field structure, for both courses of the progressive *Ra*-increasing and successive *Ra*-decreasing, are reported for the cavity with $A = 2$ in Fig. 2, where remarkable drops and rises on the *Nu*-curves may be noticed at subsequent critical Rayleigh numbers, each one corresponding to a flow-transition. In particular, the flow pattern, classified by the number of cells and by the steadiness or periodicity of the temporal asymptotic solution, evolves according to the following three-step sequence: one-cell steady → two-cell steady → two-cell oscillatory → one-to-three-cell oscillatory. Each bifurcation is then accompanied by a symmetry/asymmetry breakdown, as discussed below in details.

In the one-cell steady-state solution, the flow pattern consists of a single cell, symmetric about the center of the enclosure. In the two-cell steady-state solution, the flow pattern consists of two superimposed, counter-rotating cells, symmetric about the horizontal midplane of the enclosure. In the two-cell oscillatory solution, each of the two superimposed roll-cells expands and shrinks alternately, with no kind of spatial symmetry. Finally, in the one-to-three-cell oscillatory solution, the flow pattern becomes again symmetric about the center of the enclosure. Its evolution over one period of oscillation occurs according to the following basic sequence:

(a) starting from a single cell which occupies practically the whole cavity, the flow pattern gets progressively deformed and two secondary cells grow up at the top right and bottom left corners of the enclosure;
(b) the top and bottom cells expand along both the horizontal and vertical directions, up to reaching the dimensions of the former single cell;
(c) the top and bottom cells of the newly formed three-cell structure keep on expanding with a consequent increasing compression of the inner cell, which shrinks more and more up to vanishing;
(d) the two superimposed cells merge up to the formation of a two-in-one configuration and, subsequently, of a monocellular flow structure, specular to the starting single cell with respect to the vertical midplane of the enclosure;
(e) during the subsequent half-period, the specular flow pattern evolves according to the same sequence described above, up to the restoration of the original one-cell flow structure.

The time-evolution of the streamlines and isotherms of the one-to-three-cell oscillatory solution at $Ra = 2 \times 10^6$ is documented in Fig. 3 through six snapshots which span one half-period of oscillation. The increase in the spatio-temporal complexity with increasing the Rayleigh number is then reflected by the time-distributions of the primitive variables. As an example, the evolution of $\theta(\tau)$ vs. τ at, e.g., $X = 0.125$ and $Y = 0.25$—denoted as P in Fig. 1(b)—is shown in Fig. 4 for both the direct and the reverse courses of investigation. In particular, it may be seen that:

(a) the frequency of oscillation increases with increasing the Rayleigh number;
(b) as long as the flow-pattern type remains the same, the amplitude of oscillation keeps nearly constant with increasing/decreasing the Rayleigh number;
(c) at the same Rayleigh number, the frequency and the amplitude of oscillation of the one-to-three-cell flow pattern are respectively lower and higher than those of the two-cell flow pattern.

More details on the distributions of the dimensionless frequency vs. the Rayleigh number are reported in the window-panel of Fig. 2. From the analysis of the heat transfer results of Fig. 2, it may be noticed that each flow-transition may be accompanied or not by a more or less pronounced step change in the Nusselt number, according to whether the flow-transition is sudden, as for the first and the third bifurcations of the flow pattern evolution detailed above, or gradual, as for the second one. In particular, the flow-transition from the one-cell steady-state solution to the two-cell steady-state solution occurs with an abrupt decrease in the Nusselt number. This may easily be explained by considering that: (a) in the one-cell solution, heat is transferred across the cavity by the jet of hot fluid that, moving upwards

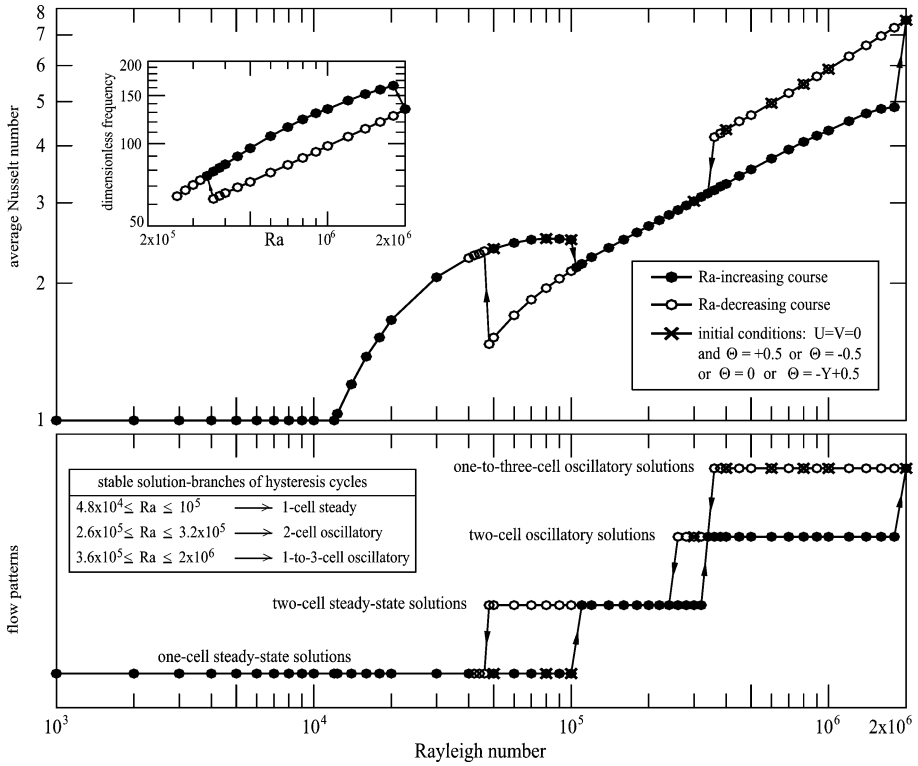

Fig. 2. Average Nusselt numbers and flow patterns vs. the Rayleigh number for $A = 2$.

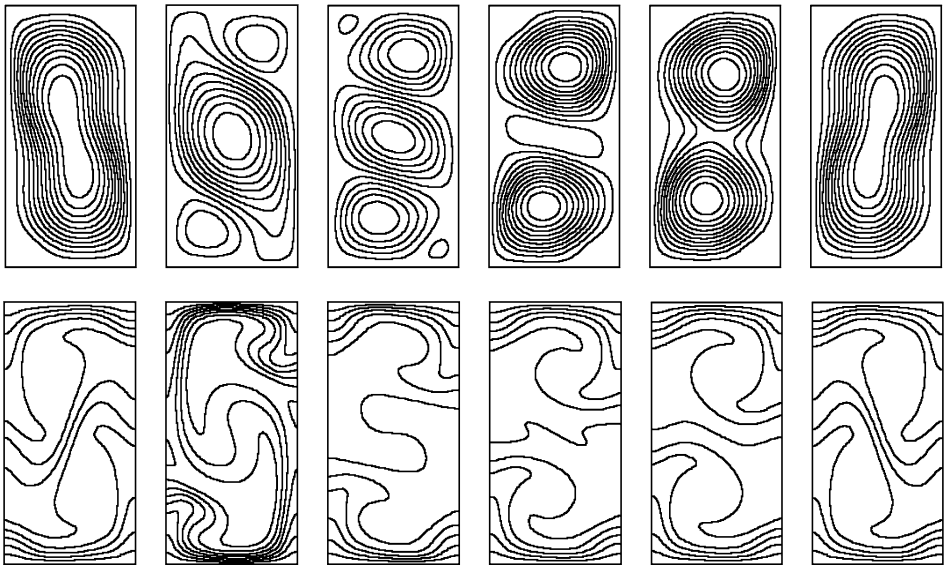

Fig. 3. Streamline and isotherm contour plots for one half-period of oscillation ($A = 2$, $Ra = 2 \times 10^6$).

along one of the sidewalls, comes directly in contact with the cooled top wall; and (b) in the two-cell solution, heat is conveyed from the bottom wall to the top wall of the cavity via the intermediate heat exchange between the horizontal fluid streams of the two superimposed rolls, which implies a smaller effectivess in the overall heat transfer. In contrast, since as said above the flow-transition from the two-cell steady-state solution to the two-cell oscillatory solution is gradual, the second bifurcation of the sequence goes along with no step change in the average Nusselt number. Finally, the third flow-transition, i.e., the bifurcation which leads from the two-cell oscillatory solution to the one-to-three-cell oscillatory solution, occurs with an abrupt increase in the Nusselt number, since the positive effect of the single cell discussed above prevails upon the significantly reduced heat transfer effectiveness of the three-cell flow pattern, which, as

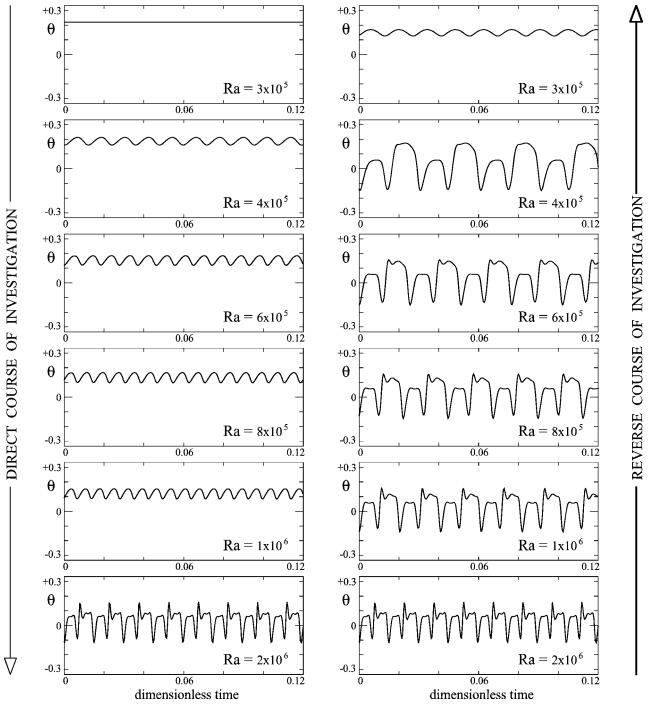

Fig. 4. Time-distributions of θ in P at subsequent Rayleigh numbers ($A = 2$).

for the two-cell configuration, is due to the intermediate heat transfers occurring between the horizontal airstreams of the three superimposed roll-cells.

In addition, the existence of a maximum on the *Nu*-curve before the first flow-transition from the one-cell steady solution to the two-cell steady solution, may be noticed. This may be ascribed to the increasing skewness of the one-cell flow pattern which, before the bifurcation, gets more and more distorted up to the separation into two superimposed cells. In fact, as *Ra* approaches the flow-transition value, the progressive distortion of the one-cell flow pattern cited above leads to a decrease in the extent of the portion of cooled top wall (or heated bottom wall) directly lapped by the jet of hot fluid moving upwards (or cold fluid moving downwards), which causes a decrease in the overall heat transfer rate.

The bifurcation sequence which developes along the reverse course, and the related drops and rises on the *Nu*-curve as well, are exactly inverted. Currently, the bifurcations along the direct and reverse courses of investigation are shifted, i.e., the critical Rayleigh numbers at which the bifurcations occur along the direct course of investigation are postponed with respect to the corresponding Rayleigh numbers of the reverse course of investigation, which reflects the tendency of the system analysed to keep memory of its thermal hystory. Hence, more or less pronounced hysteresis phenomena take place, i.e., within more or less wide ranges of variability of the Rayleigh number of the enclosure, double solutions are found.

Indeed, these double solutions have not the same physical stability, as verified through a series of tests carried out by

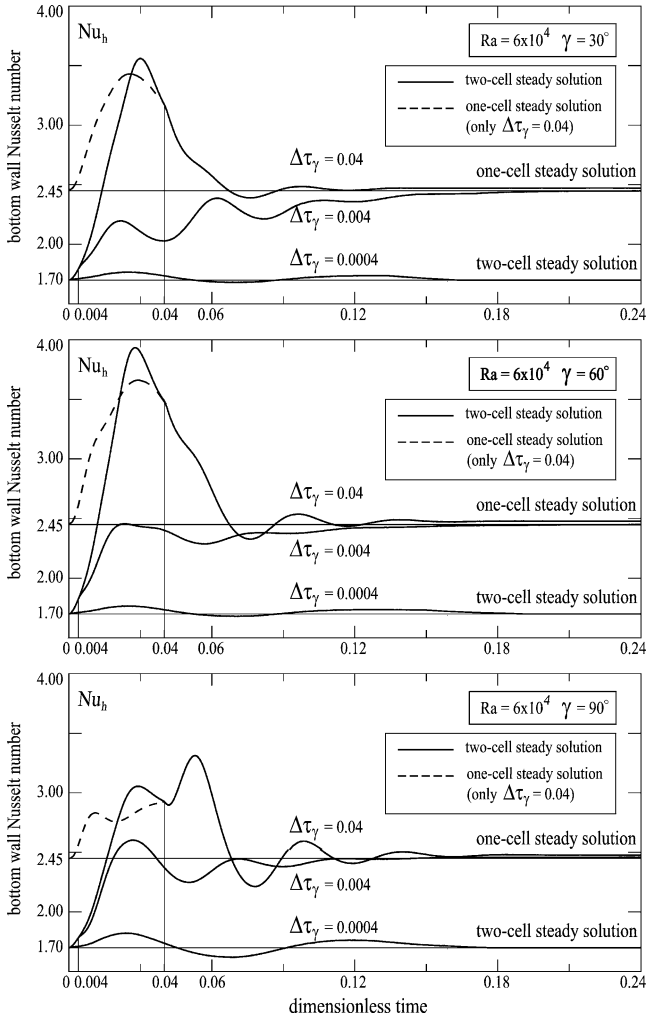

Fig. 5. Tilting effect on the one-cell and two-cell steady solutions at $Ra = 6 \times 10^4$ ($A = 2$).

tilting the enclosure of assigned angles γ for assigned time-intervals $\Delta\tau_\gamma$, and successively restoring the original upright position. Within the limits of the simulations performed, the dynamic analysis of the propagation of such disturbance throughout space and time leads to conclude that one of the solution-branches of each hysteresis cycle is represented by absolutely stable solutions, i.e., the original solution is always restored once tilting is removed. In contrast, the other solution-branch is represented by solutions with a lesser degree of stability, i.e., either the original solution or the corresponding absolutely stable solution may be reached once tilting is removed, depending on the intensity of the disturbance introduced, which means on how much the enclosure is tilted with respect to the gravity and/or on how much the duration of such tilting is long. This is illustrated in Fig. 5, where the time-distributions of Nu_h at, e.g., $Ra = 6 \times 10^4$ are reported for several combinations of γ and $\Delta\tau_\gamma$, for both the one-cell steady solution ($Nu = 2.45$) and the two-cell steady solution ($Nu = 1.70$), the latter resulting clearly much less stable than the former (indeed, since only very short tilting-times allow the two-cell system

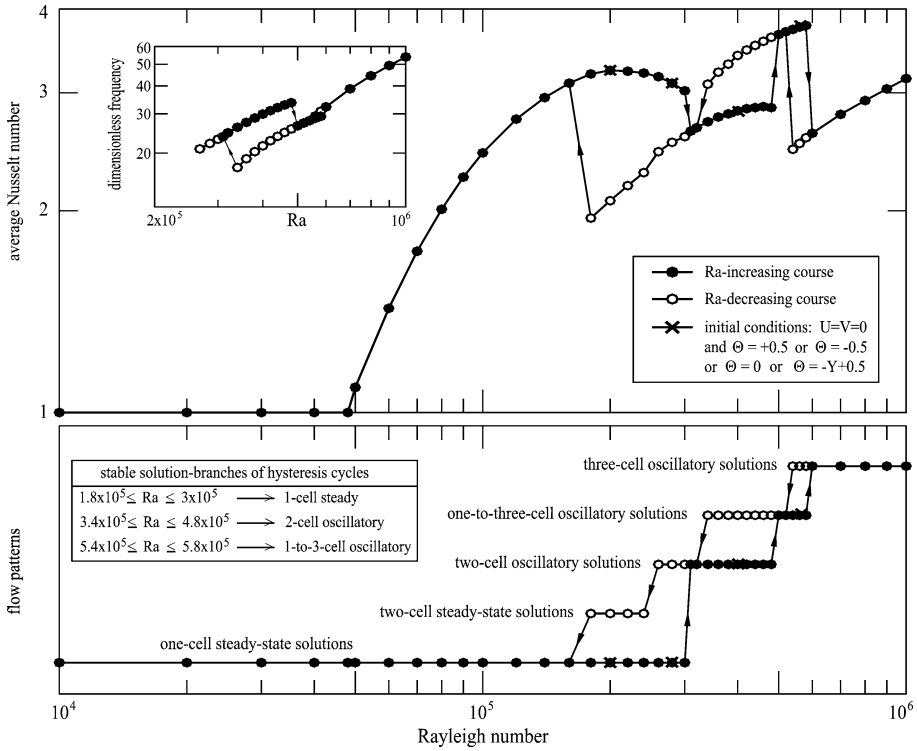

Fig. 6. Average Nusselt numbers and flow patterns vs. the Rayleigh number for $A = 3$.

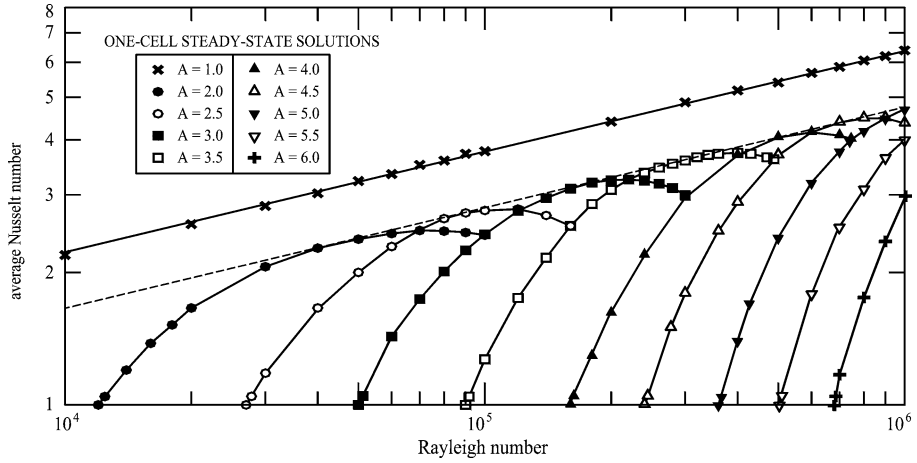

Fig. 7. Distributions of the Nusselt number vs. the Rayleigh number for the one-cell steady-state solutions.

to recover the original flow configuration, such solution can actually be denoted as a metastable solution). This differential degree of stability is also reflected by the fact that all the simulations carried out with the initial conditions of fluid at rest and temperature either uniform or varying with a linear distribution across the enclosure led to temporal asymptotic solutions that lie all on the stable solution-branch of each hysteresis cycle (see the lower panel of Fig. 2).

Same type of results found for $A = 2$ are substantially found also for the other aspect ratios investigated. The results obtained for $A = 3$ are reported in Fig. 6. In particular, it may be noticed that: (a) within the limits of the ΔRa exploratory-steps assumed, the one-cell steady solution evolves directly to the two-cell oscillatory solution, i.e., in the course of the *Ra*-increasing the two-cell steady-state flow pattern is not found (in contrast, the presence of this flow pattern is observed in the reverse course of investigation); (b) a further bifurcation, from the one-to-three-cell oscillatory solution to a more regular three-cell oscillatory solution, is found to occur with an abrupt decrease in the average Nusselt number; and (c) the maximum on the *Nu*-curve before the flow-transition from the one-cell solution to the two-cell solution is more accentuated than that observed for $A = 2$.

Other details concerning enclosures with $A > 3$ are omitted for the sake of brevity. However, since the critical Rayleigh number which corresponds to the onset of motion

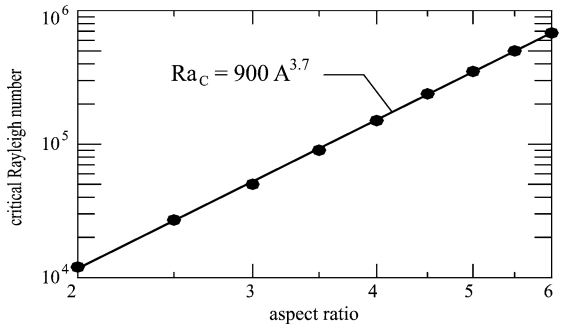

Fig. 8. Distribution of Ra_C vs. A and best-fit equation.

increases with increasing the aspect ratio of the cavity, and the upper limit of the present investigation is $Ra = 10^6$, the results relevant to enclosures with $A > 3$ which lie within this limit, are in many cases substantially limited to one-cell steady solutions. In this regard, it seems interesting to report a summary of the heat transfer rate results relevant to the only absolutely-stable, one-cell steady solutions obtained for all the aspect ratios investigated, which is plotted in Fig. 7, where the aspect ratio $A = 1$ is also included. Surprisingly, it may be noticed that: (a) the end of the *Nu*-curve of the enclosure with aspect ratio A (corresponding to the critical Rayleigh number at which the departure from the single-cell flow pattern occurs) is located at the intersection with the *Nu*-curve of the enclosure with aspect ratio $(A + 1)$; (b) the maximum of the *Nu*-curve of the enclosure with aspect ratio A is located at the intersection with the *Nu*-curve of the enclosure with aspect ratio $(A + 0.5)$; (c) in the double-Log plane *Nu*–*Ra*, all the *Nu*-curves have a unique tangent-line, which is parallel to the straight line of interpolation of the results obtained for the enclosure with aspect ratio $A = 1$. In addition, the first critical Rayleigh number Ra_C at which the departure from motionless conduction occurs, may be expressed as a simple function of the aspect ratio A through the best-fit correlation-equation represented in Fig. 8:

$$Ra_C = 900A^{3.7} \tag{11}$$

with a standard deviation of data $\sigma = 0.016$ and a maximum value of the absolute maximum error $\varepsilon = 0.03$.

5. Conclusions

Rayleigh–Bénard convection in air-filled, rectangular enclosures with adiabatic sidewalls has been studied numerically for height-to-width aspect ratios of the cavity in the range 2 to 6, by progressively increasing and successively decreasing the Rayleigh number based on the height of the cavity in the range 10^3 to 2×10^6.

In particular, as *Ra* is increased through a step-by-step procedure, the flow pattern evolves according to the following general sequence: one-cell steady → two-cell steady → two-cell periodic → one-to-three-cell periodic → three-cell periodic. An exactly inverted bifurcation sequence has been detected along the reverse *Ra*-decreasing course of investigation. Indeed, for $A \geqslant 3$, in the course of *Ra*-increasing the flow pattern has been found to evolve directly from the one-cell steady solution to the two-cell oscillatory solution.

Each bifurcation is then accompanied by a symmetry/asymmetry breakdown. Even more important, each bifurcation is accompanied by a more or less pronounced step-change in the Nusselt number, as well as by a hysteresis cycle, whose solution-branches are found to be characterized by a differential degree of stability.

Finally, the *Nu*-curves for the single-cell steady-state solutions show some surprising modular peculiarities which, in our opinion, deserve further investigation.

References

[1] G.D. Raithby, K.G.T. Holland, Natural convection, in: W.M. Rosenhow, J.P. Hartnett, E.N. Ganic (Eds.), Handbook of Heat Transfer Fundamentals, second ed., McGraw-Hill, New York, 1985, Chapter 6.
[2] J.P. Gollub, S.V. Benson, Many routes to turbulent convection, J. Fluid Mech. 100 (1980) 449–470.
[3] A. Libchaber, C. Larouche, L. Fauve, Periodic doubling cascade in mercury, a quantitative measurement, J. Phys. Lett. 43 (1982) L211–L216.
[4] D. Mukutmoni, K.T. Yang, Rayleigh–Bénard convection in a small aspect ratio enclosure, Part I—Bifurcation to oscillatory convection, J. Heat Transfer 115 (1993) 360–366.
[5] D. Mukutmoni, K.T. Yang, Rayleigh–Bénard convection in a small aspect ratio enclosure, Part II—Bifurcation to chaos, J. Heat Transfer 115 (1993) 367–376.
[6] D. Mukutmoni, K.T. Yang, Thermal convection in small enclosures: An atypical bifurcation sequence, Internat. J. Heat Mass Transfer 38 (1995) 113–126.
[7] J.R. Leith, Successive transitions of steady states in moderate size containers of air heated from below and cooled above, in: Bifurcation Phenomena in Thermal Processes and Convection, in: HTD, vol. 94, 1987.
[8] R. Hernandez, R.L. Frederick, Spatial and thermal features og three dimensional Rayleigh–Bénard convection, Internat. J. Heat Mass Transfer 37 (1994) 411–424.
[9] K.T. Yang, Transitions and bifurcations in laminar buoyant flows in confined enclosures, J. Heat Transfer 110 (1988) 1191–1204.
[10] E.L. Koschmieder, Bénard Cells and Taylor Vortices, Cambridge Univ. Press, Cambridge, 1993.
[11] A.V. Getling, Rayleigh–Bénard Convection: Structures and Dynamics, World Scientific, Singapore, 1997.
[12] A.Y. Gelfgat, Different modes of Rayleigh–Bénard instability in two- and three-dimensional rectangular enclosures, J. Comput. Phys. 156 (1999) 300–324.
[13] J. Pallares, I. Cuesta, F.X. Grau, F. Giralt, Natural convection in a cubical cavity heated from below at low Rayleigh numbers, Internat. J. Heat Mass Transfer 39 (1996) 3233–3247.
[14] J. Pallares, F.X. Grau, F. Giralt, Flow transitions in laminar Rayleigh–Bénard convection in a cubical cavity at moderate Rayleigh numbers, Internat. J. Heat Mass Transfer 42 (1999) 753–769.
[15] J.P. Van Doormaal, G.D. Raithby, Enhancements of the simple method for predicting incompressible fluid flows, Numer. Heat Transfer 17 (1984) 147–163.
[16] S.V. Patankar, D.B. Spalding, A calculation procedure for heat, mass and momentum transfer in three-dimensional parabolic flows, Internat. J. Heat Mass Transfer 15 (1972) 1787–1797.
[17] S.V. Patankar, Numerical Heat Transfer and Fluid Flow, Hemisphere, Washington, DC, 1980.

[18] S.V. Patankar, Recent developments in computational heat transfer, J. Heat Transfer 110 (1988) 1037–1045.
[19] G. de Vahl Davis, Natural convection of air in a square cavity: A bench mark numerical solution, Internat. J. Numer. Meth. Fluids 3 (1983) 249–264.
[20] H.S. Mahdi, R.B. Kinney, Time-dependent natural convection in a square cavity: Application of a new finite volume method, Internat. J. Numer. Meth. Fluids 11 (1990) 57–86.
[21] M. Hortmann, M. Peric, G. Scheuerer, Finite volume multigrid prediction of laminar natural convection: Bench-mark solutions, Internat. J. Numer. Meth. Fluids 11 (1990) 189–207.
[22] O. Aydin, Transient natural convection in rectangular enclosures heated from one side and cooled from above, Internat. Comm. Heat Mass Transfer 26 (1999) 135–144.